Photochemical Deposition of ZnS from the Gas Phase and Simultaneous Luminescence Detection of Photofragments from a Single-Source Precursor, $Zn(S_2COCHMe_2)_2$

Jinwoo Cheon, David S. Talaga, and Jeffrey I. Zink*

Contribution from the Department of Chemistry and Biochemistry, University of California, Los Angeles, Los Angeles, California 90095

Received July 26, 1996[⊗]

Abstract: ZnS thin films are made by laser driven chemical vapor deposition (CVD) from a single-source precursor, $Zn(S_2COCHMe_2)_2$ under vacuum conditions. Photofragments in the gas phase are identified simultaneously by luminescence spectroscopy. The laser selectively activates the initial decomposition of the precursor and drives its conversion to the desired materials under mild conditions. These photolytically produced films are compared to films made by thermal deposition from the same precursor. The deposits from both techniques, characterized by X-ray diffraction, Rutherford backscattering, and X-ray photoelectron spectroscopy, are pure stoichiometric ZnS in the hexagonal phase. Surface morphology differs in shape and granule size. During the laser-driven CVD process, gas-phase photochemical intermediates are identified by luminescence spectroscopy. The luminescent photoproducts are Zn and S_2, the two elemental components of the final material. Photofragmentation mechanisms leading to ZnS, the luminescent species Zn and S_2, and the gaseous organic byproducts are discussed. Further characterization of the photofragmentation pathways is provided by the trapping of the photoreaction products and by mass spectroscopy.

Introduction

Photochemical applications for materials synthesis and modification have been extensively studied.[1−7] In particular, for the preparation of thin film materials, laser assisted chemical vapor deposition (CVD) processes have the advantages of spatial selectivity of deposition on the substrate, selective energy transfer to the deposition precursor, and low processing temperatures.[8−10] Efforts to fabricate multilayer structures with well-defined physical properties and abrupt interfaces benefit from the low growth temperatures. With this technique, patterned features of the desired materials can be drawn in "real time" in a one- or two-step process compared with the many steps involved in current lithographic techniques. Under photochemically driven CVD conditions, luminescence may be observed, and luminescence spectroscopy can then identify photofragments and assist in the elucidation of the photolytic deposition pathways. The effects of changing the deposition conditions can be determined by observing the corresponding changes in the spectra. In addition, luminescence spectroscopy can determine product internal energies and relaxations that are important to explain the laser deposition process. We have previously used these techniques to study the laser driven photochemical CVD processes from copper and gold hexafluoroacetylacetonate compounds.[11,12] "Real time" chemical information about activated gas-phase species involved in materials growth on substrates is difficult to obtain but is very important for better understanding and improving the CVD process.

Important objectives for laser-assisted CVD are wide-band-gap semiconductors. Intensive research on the growth of wide-band-gap films has included use of pyrolytic CVD,[13,14] pulsed laser ablation,[15] and molecular beam epitaxy (MBE).[16] For example, ZnS and ZnSe are currently used as emitting layers in electroluminescent devices and have potential for blue region light emitting diode and laser optoelectronic applications.[17−20] ZnS has a direct band gap of 3.7 eV. Conventional thermolytic MOCVD of ZnS from dual source precursors (e.g. $ZnMe_2$ and H_2S) frequently suffers from such problems as premature reactions between the precursors and high process temperatures,[21] resulting in poor quality inhomogeneous films.[22] MBE techniques suffer difficulties with stoichiometry control, particularly with respect to sulfur.[23] In this paper, we explore the use of a single-source precursor. Research on single-source precursors has been very active and there are examples of this

[⊗] Abstract published in *Advance ACS Abstracts,* December 1, 1996.

(1) Avey, A. A.; Hill, R. H. *J. Am. Chem. Soc.* **1996**, *118*, 237.
(2) Doppelt, P.; Baum, T. H. *MRS Bull.* **1994**, *19*, 41.
(3) Larciprete, R. *Appl. Surf. Sci.* **1990**, *46*, 19.
(4) Lee, E. J.; Bitner, T. W.; Ha, J. S.; Shane, M. J.; Sailor, M. J. *J. Am. Chem. Soc.* **1996**, *118*, 5375.
(5) Bhatia, S. K.; Hickman, J. J.; Ligler, F. S. *J. Am. Chem. Soc.* **1992**, *114*, 4432.
(6) Dressick, W. J.; Dulcey, C. S.; Georger, J. H., Jr.; Calvert, J. M. *Chem. Mater.* **1993**, *5*, 148.
(7) Moreau, W. M. *Semiconductor Lithography; Principles, Practices, and Materials*; Plenum: New York, 1988.
(8) Kompa, K. L. *Angew. Chem., Int. Ed. Engl.* **1988**, *27*, 1314.
(9) Herman, I. P. *Chem. Rev.* **1989**, *89*, 1323.
(10) Eden, J. G. *Photochemical Vapor Deposition*; Wiley: New York, 1992.
(11) Wexler, D.; Zink, J. I.; Tutt, L. W.; Lunt, S. R. *J. Phys. Chem.* **1993**, *97*, 13563.
(12) Talaga, D. S.; Zink, J. I. *Inorg. Chem.* **1996**, *35*, 5050.
(13) Li, J. W.; Su, Y. K.; Yokoyama, M. *Jpn. J. Appl. Phys.* **1996**, *35*, 5050.
(14) Smith, P. B. *J. Vac. Sci. Technol. A* **1989**, *7*, 1451.
(15) Mclaughlin, M.; Sakeek, H. F.; Maguire, P.; Graham, W. G.; Molloy, J.; Morrow, T.; Laverty, S.; Anderson, J. *Appl. Phys. Lett.* **1993**, *63*, 1865.
(16) Kitagawa, M.; Tomomura, Y.; Nakanishi, K.; Suzuki, A.; Nakajima, S. *J. Cryst. Growth* **1990**, *101*, 52.
(17) Yamaga, S. *Jpn. J. Appl. Phys.* **1991**, *30*, 437.
(18) Neumark, G. F.; Park, R. M.; Depuydt, J. M. *Physics Today* **1994** (June), 26.
(19) Ohring, M. *The Materials Science of Thin Films*; Academic: San Diego, 1992.
(20) McClean, I. P.; Thomas, C. B. *Semicond. Sci. Technol.* **1992**, *7*, 1394.
(21) Kukimoto, H. *J. Cryst. Growth* **1991**, *107*, 637.
(22) Giapis, K. P.; Jensen, K. F.; Potts, J. E.; Pachuta, S. J. *J. Electron. Mater.* **1990**, *19*, 453.
(23) Ando, H.; Taike, A.; Konagai, M.; Takahashi, K. *J. Appl. Phys.* **1987**, *62*, 1251.

S0002-7863(96)02589-9 CCC: $14.00

approach for the deposition of binary III/V (e.g. GaAs)[24,25] and II/VI (e.g. ZnSe)[26] semiconductor materials.

In this paper, we focus on ZnS and the laser-driven CVD from a single-source precursor. We simultaneously study the gas-phase luminescence during the CVD process to elucidate the laser-driven fragmentation pathways. This study is one of the first demonstrations of the simultaneous utilization of a laser for both initiating and characterization in materials synthesis. We choose an air-stable zinc compound with a sulfur chelating ligand, zinc xanthate, bis(*O*-isopropyldithiocarbonato)zinc(II), $Zn(S_2COCHMe_2)_2$, as our CVD precursor. The metal coordination sphere only contains sulfur, and we show that the molecule is photochemically activated in the gas phase to give ZnS. As part of this study we examine the material produced by the thermal CVD process and compare it with the photolytically-produced material.

Experimental Section

General Methods. The precursor, $Zn(S_2COCHMe_2)_2$, was prepared by the stoichiometric reaction of potassium isopropylxanthate and zinc nitrate following the literature method.[27] The thin film stoichiometry was determined by Rutherford backscattering spectroscopy (RBS) using a 1.8 MeV He ion beam with a silicon surface barrier detector located at 165° with respect to the ion beam. X-ray powder diffraction (XRD) patterns were acquired using Cu Kα radiation with a power supply of 40 KV and 30 mA. Scanning electron micrographs were obtained on a Cambridge Stereo Scan 250 instrument. X-ray photoelectron spectra were obtained with a 15 KV, 400 W Al Kα radiation source (1486.6 eV) under an operation pressure of ca. 10^{-10} Torr. In the case of the GC/MS analysis of the organic byproducts during photo-CVD, trapped gaseous samples (100 μL) were injected into a heated GC injection port (150 °C) of a modified Hewlett-Packard 5985B gas chromatograph equipped with a medium polarity fused silica capillary column (0.25 mm × 30 m, DBS, J&W Assoc.). The end of the column was inserted directly into the electron ionization (70 eV) source of a quadruple mass spectrometer. The GC/MS transfer line was held at 150 °C and the mass spectrometer was scanned from *m*/*z* 20 to 200.

Mass Spectroscopy. Laser desorption/ionization mass spectra were acquired by inserting a powdered sample on a stainless steel surface into an ionization chamber (~10^{-5} Torr) of a Per Septive Biosystems Voyager RP LD TOF instrument. A nitrogen laser (337 nm) ablates and ionizes the precursor, $Zn(S_2COCHMe_2)_2$, and time of flight (TOF) mass spectra were obtained by positive and negative ion modes. Major species identified (*m*/*z*): SO base peak at 48 (100%), S 32 (90%), $CHMe_2$ 43 (93%), CS_2 76 (32%), ^{64}ZnS 96 (18%), $Me_2CH\text{-}S\text{-}CHMe_2$ 118 (19%), Me_2CHOCS_2H 136 (26%), $Me_2CHOCS_2CHMe_2$ 178 (21%), $^{64}Zn(S_2COCHMe_2)S$ 231 (24%), $^{64}Zn(S_2COCHMe_2)_2$ 334 (10%).

High-resolution electron ionization (70 eV) mass data of the precursor, $Zn(S_2COCHMe_2)_2$, were recorded on a VG Autospec mass spectrometer. The mass spectrometer was scanned from *m*/*z* 80 to 600 at a resolution of about 10 000 ($M/\Delta m$, 10% valley) using perfluoro kerosene as the internal calibrant. Major species identified (*m*/*z*): $^{64}Zn(S_2COCHMe_2)_2$ base peak at 334 (100%), ^{64}ZnS 96 (23%), $S_2COCHMe_2$ 135 (57%), $^{64}Zn(S_2COCHMe_2)$ 199 (14%), $^{64}Zn(S_2COCHMe_2)$ S 231 (14%), [bimetallic species: $^{64}Zn(S_2COCHMe_2)_2 + {}^{64}ZnS$] 430 (2%), [bimetallic species: $^{64}Zn(S_2COCHMe_2)_2 + {}^{64}Zn(S_2COCHMe_2)_1$] 533 (3%).

Thermal CVD. The thermal-CVD experiments were conducted at ~10^{-2} Torr in a hot wall horizontal Pyrex tube where two different temperature regions (sublimation and deposition) are regulated by external heating tape. The precursor (~0.1 g) was slowly sublimed at 120 °C into the film growth region and deposition occurred at 350 °C on the substrates used (Si wafers, quartz slides) as well as on the inner surface of the reactor wall. The films grown were reflective. During the CVD experiments, exhaust gases were collected in a liquid nitrogen cold trap. The organic byproducts collected were analyzed by GC/MS. The major components are propene, OCS, RSR, and RSH (R = $CHMe_2$). Typical deposition times were about 2 h, and ~400 nm thick films were obtained.

Photolytic CVD. Laser driven photodeposition was carried out using a XeCl excimer laser (308 nm) at ~10^{-2} Torr. The zinc xanthate precursor (~0.1 g) in a reservoir cell was heated to sublimation temperature (120 °C) and introduced into a CVD glass cell with quartz windows. The photodeposition was carried out by irradiating a 2 cm diameter circle on substrates (Si wafers, quartz slides) with approximately 30 mJ/pulse at 20 Hz for a resulting fluence of ~1 MW cm^{-2}. During the CVD experiments, exhaust gases were collected in a liquid nitrogen cold trap. The organic byproducts collected were analyzed by GC/MS. The major components are RH, ROH, CS_2, OCS, RSR, and RSH (R = $CHMe_2$). Typical deposition times were about 2 h, and ~100 nm thick films were obtained.

Luminescence Spectroscopy. Luminescence experiments are carried out in an evacuated stainless steel 6-way cross with synthetic fused silica windows. A sample of the CVD precursor is placed in the sample chamber and is leaked into the photolysis chamber with a needle valve. Buffer gases can be introduced both *via* a separate inlet and optionally in conjunction with the sample. Luminescence spectra are obtained under a variety of pressure conditions [e.g. dynamic vacuum (10^{-2} Torr), static vacuum, Ar buffer gas (~1−1000 Torr)]. The entire cell is heated using thermostated heating tape. The light source for our spectroscopic investigations is a Lambda Physik EMG 201 MSC XeCl excimer laser. The pulse width is typically 12 ns. The 308 nm pulse energy used for excitation of the CVD precursors is approximately 3 mJ. The excimer laser is focused with a $\phi = 1$ in. $f = 50$ mm CaF lens. The resulting fluence is typically ~3 MW/cm^2. The focused output of the laser excites the gaseous sample and the emitted light is collected by *f*/4 optics at right angles and directed into a 0.32 m single monochromator (JY HR320) where it is dispersed by a 300 or 600 groove/mm holographic grating and detected by an UV intensified diode array detector (EG&G Princeton Applied Research OMA3 1024×1). Resolution is determined by the grating dispersion and the element spacing on the array detector. The spectral width of a pixel is ~0.24 nm and ~0.12 nm for the 300 and 600 groove/mm gratings, respectively. The UV intensifier allows time resolved gating of the detector with a resolution of 10 ns.

Results and Discussion

1. CVD Studies. (a) Thermal CVD. Shiny films of pure ZnS were grown on silicon wafers and glass substrates from the zinc xanthate precursor by thermal CVD. The deposition zone was maintained at 350 °C under vacuum (10^{-2} Torr). The reflective films were characterized by four surface analytical methods. The Zn and S atomic concentrations and the purity of the ZnS films were investigated by using the techniques of Rutherford Backscattering (RBS) and X-ray photoelectron spectroscopy (XPS). RBS yields elemental information representative of the entire thickness of the film, with a quantitative accuracy estimated at ±5%. XPS was used to verify the near-surface composition, as XPS samples only the top few molecular layers. Our RBS data from films grown on Si wafer indicate a 1:1 ratio of Zn:S within the accuracy of the technique. Surface XPS scans after Ar^+ ion sputtering of the surface for 3 min reveal only trace amounts of carbon and oxygen contamination (≤~4%) on the ZnS films. The unsputtered surface contained large amounts of adsorbed carbon (~20%) and oxygen (~20%) that are attributed to air exposure and handling of the films following growth.

X-ray diffraction (XRD) studies of the films indicate that they are comprised of polycrystalline ZnS. The peaks from the hexagonal (α) and cubic (β) phases of ZnS overlap considerably. In order to differentiate between them the presence of the (100) peak at $2\theta = 27°$ is taken as evidence for the existence of the

(24) Cowley, A. H.; Jones, R. A. *Angew. Chem., Int. Ed. Engl.* **1989**, *28*, 1208.
(25) Zanella, P.; Rossetto, G.; Brianese, N.; Ossola, F.; Porchia, M.; Williams, J. O. *Chem. Mater.* **1991**, *3*, 225.
(26) O'Brien, P.; Nomura, R. *J. Mater. Chem.* **1995**, *5*, 1761.
(27) Rao, S. R. *Xanthate and Related Compounds*; Dekker: New York, 1971.

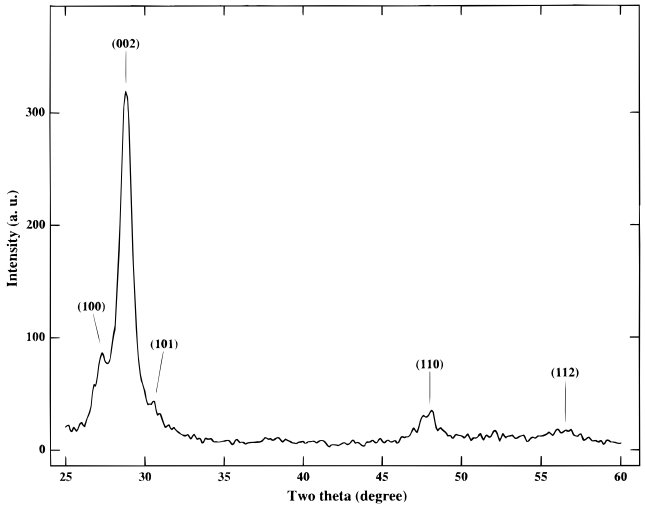

Figure 1. X-ray diffraction pattern of hexagonal (α) phase ZnS grown at 350 °C by thermal CVD.

hexagonal structure.[28] Strong preferred orientation at $2\theta = 28.56°$ due to hexagonal (002) is observed (Figure 1). This preferential growth pattern has been reported in other studies.[29]

Scanning electron microscopy showed that ZnS films grown on Si wafers at 350 °C are rather smooth, but consist of large grains (∼10 μm in diameter) (Figure 2a).

(b) Photolytic CVD. To prevent any possible condensation of the precursor, the film growth cell was kept at 120 °C, while the substrate was irradiated with a laser beam ∼2 cm in diameter. Under laser driven deposition conditions, smooth and reflective deposits were formed on the Si wafer and glass slide substrates only where the laser irradiated substrate. Deposition also occurred on the top quartz cell window where the laser beam entered the cell.

The photodeposited films were characterized by surface analytical techniques. RBS analysis (Figure 3) showed that the films have almost stoichiometric ZnS composition. A slight excess of sulfur (∼5 atom %, $Zn_{1.0}S_{1.07}$) may be present, but it is just outside of the experimental uncertainty. XPS analysis of the film reveals that the ZnS surface contains only trace amounts of carbon and oxygen contamination (≤∼4%) after sputtering with Ar^+ for 3 min. No other impurities are detected in the film (Figure 4). XRD analyses show that the films are hexagonal phase polycrystalline ZnS. We did not observe any epitaxial growth nor substrate dependent ZnS growth pattern in the photolytically-produced films.

SEM revealed that the film consists of small granular particles (∼1 μm in diameter) (Figure 2b). The grain sizes are about 10 times smaller than those in the thermally-produced films. In the thermally grown films, much larger grain boundaries are possibly formed because of the higher surface mobility at the higher substrate temperature.[19] It has been previously demonstrated that the grain size of ZnS increases with the growth temperature.[14] These experimental results do not conclusively rule out the possibility of a thermal CVD component caused by laser heating of the substrates. However, the similarity of the deposition process on quartz (which does not strongly absorb the laser light) and on the Si wafer, suggests that heating alone is not the sole cause of the deposition. The photofragmentation study discussed below shows that the process depends on the absorption of light and involves a photochemical component.

(28) *JCPDS Powder Diffraction File*; McClune, W. F., Ed.; International Center for Diffraction Data: Swarthmore, PA, 1990.

(29) Fang, J.; Holloway, P. H.; Yu, J. E.; Jones, K. S.; Pathangey, B.; Brettschneider, E.; Anderson, T. J. *Appl. Surf. Sci.* **1993**, *70/71*, 701.

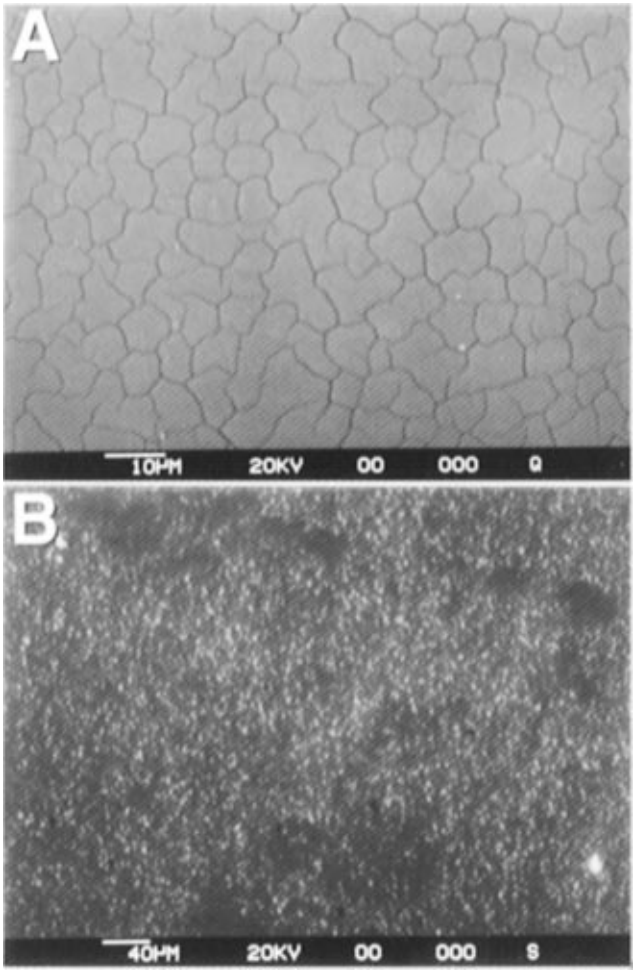

Figure 2. Scanning electron micrographs of ZnS films grown on Si(100) by (a) thermal and (b) photolytic CVD.

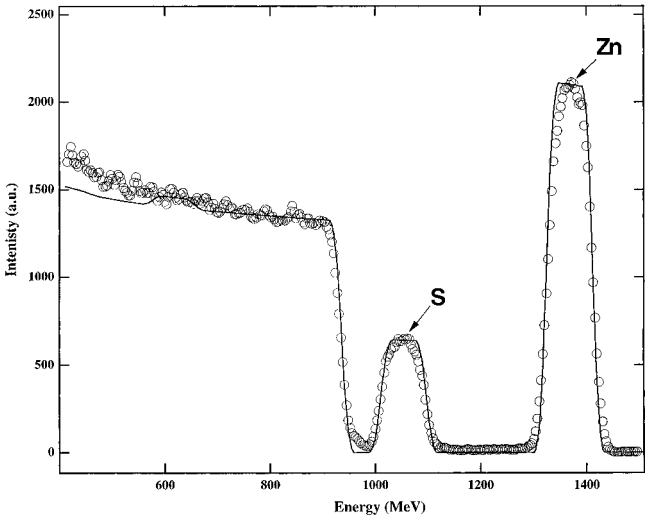

Figure 3. Rutherford backscattering of ZnS deposited on Si(100) by photolytic CVD. Data fitting was carried out using RUMP simulation for a Zn:S ratio of 1:1.07.

2. Luminescence of Photofragments. During the course of the laser-assisted CVD studies, we observe luminescence in the path of the laser beam in the cell Because the luminescence spectra provide the opportunity to identify the chemcial species giving rise to the emission under exactly the same conditions as those used for photodeposition, a spectroscopic study was undertaken. The emission spectra show that the luminescence originates from gas-phase photofragments and not from the

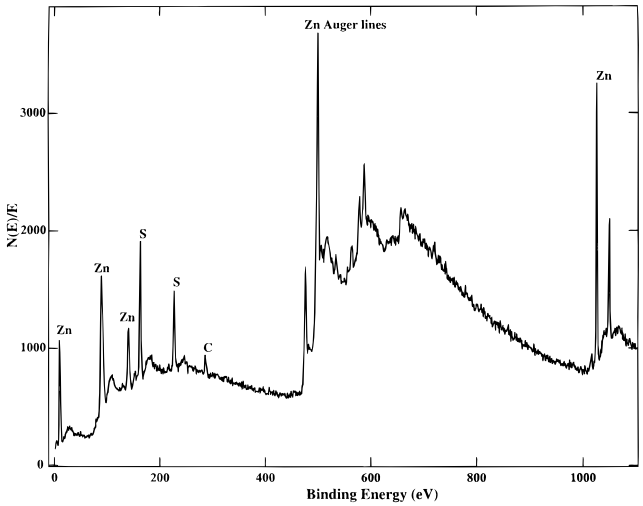

Figure 4. X-ray photoelectron spectrum of ZnS grown on Si(100) by photolytic CVD.

intact precursor molecule. By using gating techniques to separate the spectra of short- and long-lived species, it is possible to identify many of the photofragments and to use the information to develop an understanding of the photofragmentation pathways.

The luminescence spectrum observed during the deposition process is shown in Figure 5A and exhibits two main features. These are separted by time-resolved gated experiments. Under low-pressure conditions three sharp bands appear at 468.0, 472.2, and 481.1 nm due to Zn atomic emission (Figure 5B). Less intense broader, regularly spaced bands (~720 cm^{-1} spacing) from 310 to 570 nm are observable in the gated spectra and are assignable to vibrationally hot S_2 as shown in the top trace of Figure 5C. The top trace of Figure 5D shows that the time-resolved spectrum in the presence of added argon buffer gas (~200 mbar) contains a congested progression from 340 to 500 nm which is also assignable to S_2. The bottom trace of Figure 5D shows a simulated S_2 emission spectrum which matches well with the observed S_2 luminescence.

We originally anticipated that we might see luminescence from ZnS(g) since the precursor deposits bulk ZnS. ZnS(g) has two absorption bands in the UV, but both of them are unstructured implying that the excited states are dissociative.[30] Therefore we do not expect that any excited state ZnS(g) that is formed would exhibit luminescence. Moreover, it should fragment producing Zn* and S, which is consistent with the spectra we observe.

3. Photofragmentation Pathways. To further characterize the gas-phase fragmentation pathways, we examine the laser desorption/ionization mass spectra, electron ionization mass spectra, and photoproducts from the deposition process that are trapped at liquid nitrogen temperature. This information, combined with the identification of the luminescent photofragments discussed above, allows elucidation of the fragmentation mechanisms leading to the deposition of ZnS. In the following sections, we discuss the fragmentation leading to the luminescent species, fragmentation leading to ZnS, and fragmentation leading to the other major species observed in the trapping and mass spectroscopy experiments.

(a) Fragmentation Leading to the Luminescent Species. The first step of this fragmentation process is a ligand-to-metal charge transfer (LMCT), which generates $Zn(S_2COCHMe_2)$ and a xanthate radical (Path A of Figure 6). Both of these fragments

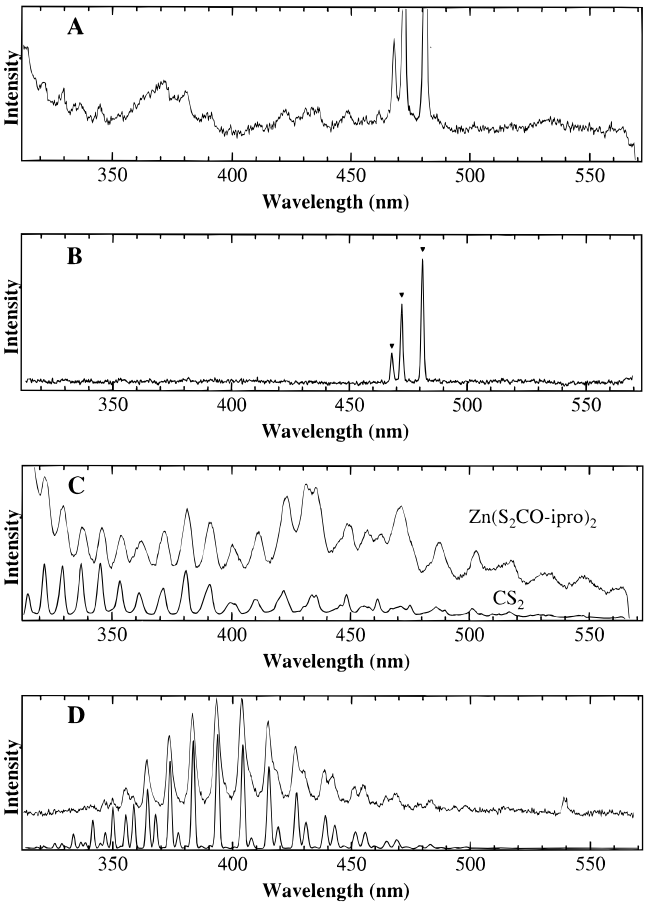

Figure 5. (A) *In situ* luminescence spectrum observed during photolytic CVD of $Zn(S_2COCHMe_2)_2$. (B) Gated spectrum observed under low-pressure conditions for the 10 ns during the laser pulse. Positions of known Zn atomic emission lines are shown with triangles. (c) The upper trace is the spectrum observed under low-pressure conditions delayed 30 ns after the laser pulse and integrated for 40 ns thereafter (hot S_2 emission). The lower trace is the spectrum observed from CS_2 under identical photolytic CVD conditions. (D) The upper trace shows the spectrum observed under high-pressure conditions delayed 80 ns after the laser pulse and integrated for 10 μs thereafter (collisionally cooled S_2 emission). The lower trace shows a simulated spectrum of the S_2 B $\rightarrow$ X luminescence including contributions from the $\nu = 0$, 1, 2 bands in the excited state.

are major species in the electron impact mass spectrum. Analogous photoactivated ligand dissociation processes that involve homolytic cleavage of the M−S bond and formation of free ligand have been reported for metal dithiocarbamate complexes.[31,32] Further photofragmentation of the photointermediate $Zn(S_2COCHMe_2)$ produces another xanthate radical and a zinc atom (Path B of Figure 6). The luminescence of the zinc atoms probably occurs because they are produced in excited electronic states. Atomic zinc does not have absorption lines at 308 nm and thus cannot be excited directly by the laser.

The emission from S_2 arises from further fragmentation steps involving the xanthate radical. The xanthate radical ($^{\bullet}S_2COCHMe_2$) can fragment yielding CS_2 and an isopropoxy radical (Path C of Figure 6). Absorption of a UV photon by CS_2 results in fragmentation yielding CS and S. The S atom can further react with CS_2 to produce luminescent S_2.[33] CS_2 is observed in the laser desorption mass spectra as are S atoms.

(30) Pearse, R. W. B.; Gaydon, A. G. *The Identification of Molecular Spectra*; Chapman and Hall: London, 1976.

(31) Schwendiman, D. F.; Zink, J. I. *J. Am. Chem. Soc.* **1976**, *98*, 4439.

(32) Given, K. W.; Mattson, B. M.; McGuiggan, M. F.; Miessler, G. L.; Pignolet, L. H. *J. Am. Chem. Soc.* **1977**, *99*, 4855.

(33) Sapers, S. P.; Andraos, N.; Donaldson, D. J. *J. Chem. Phys.* **1991**, *95*, 1738.

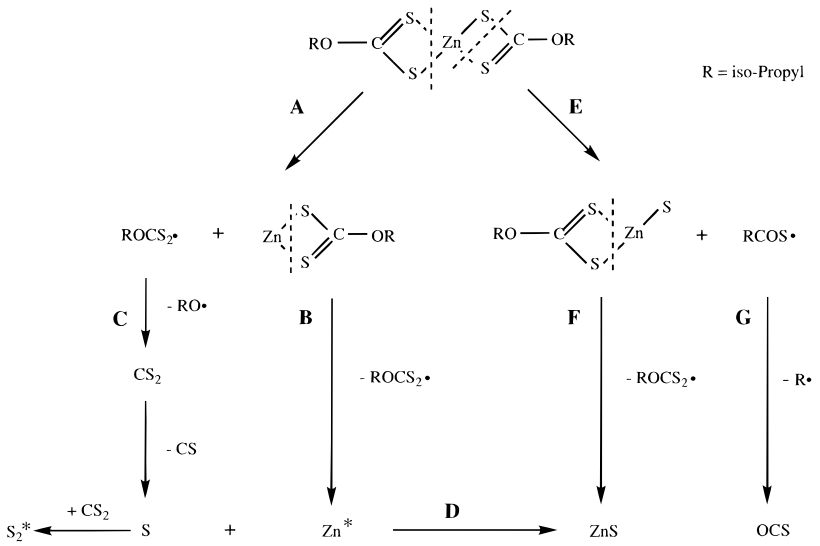

Figure 6. Photochemically activated fragmentation processes of $Zn(S_2COCHMe_2)_2$ which lead to solid ZnS and to gas-phase Zn atom and S_2 luminescence.

The low-pressure spectrum of zinc xanthate shows features assignable to very hot S_2 ($B \rightarrow X$).[30] Our photofragmentation control study of CS_2 under identical conditions to those used for the zinc xanthate complex reproduces all of the non-zinc features present in the zinc xanthate photofragmentation spectrum which are assigned to S_2 (Figure 5C). A similar control study of OCS did not give S_2 emission. The spectrum from S_2 observed under higher pressure conditions with added Ar buffer gas shows substantial cooling as a result of collisions (Figure 5D). Therefore, we conclude that CS_2 is a photofragment of the zinc xanthate complex. This photoproduct is indicative of complete ligand loss followed by C−O bond cleavage to produce both CS_2 and an isopropoxy radical (Path C). Loss of a second intact ligand (Path B) would produce zinc atoms, consistent with the spectra we observe in the gas phase. However, as we will discuss later, mass spectral evidence shows that loss of the second ligand may not be the exclusive pathway.

(b) Fragmentation Leading to ZnS. ZnS is produced by a variety of routes. One of the pathways is implied by the luminescence identification of zinc and sulfur. Combination of these atoms in the gas phase or on the surface leads directly to deposition of the ZnS film (Path D of Figure 6).

A second pathway is illustrated on the right side of Figure 6. The first step in this process is the loss of ROCS to produce $LZnS$ ($L = S_2COCHMe_2$), i.e. ZnS coordinated by one xanthate ligand (Path E). This species is a major component in the electron impact and laser desorption TOF mass spectra. Photolytic loss of the xanthate ligand from this species, either in the gas phase or on the surface, produces ZnS (Path F).

(c) Fragmentation Leading to Other Major Species. The electron impact mass data show that the molecular ion $[Zn(S_2COCHMe_2)_2]^+$ is the strongest peak, which implies that the precursor molecule exists as a monomer in the gas phase. We also identified many cracking fragments with the major species being a free xanthate ligand ($S_2COCHMe_2$), a one-ligand complex $Zn(S_2COCHMe_2)$, and a three-coordinate complex $Zn(S_2COCHMe_2)S$. Minor species include a three-ligand bimetallic complex $[Zn(S_2COCHMe_2)_2 + Zn(S_2COCHMe_2)_1]$, and another three-ligand bimetallic molecule $[Zn(S_2COCHMe_2)_2 + ZnS]$. These results show that the metal ligand (Zn−S) bond and the S−C bond of the ligand are weak. Also, these results suggest that the bonds that are marked by dotted lines in Figure 6 are relatively weaker than others and Paths A and E are the most important during initial photofragmentation.

The laser desorption mass spectroscopy studies show highly fragmented species from the zinc xanthate compounds. In this process, the precursor was ablated and ionized by N_2 laser irradiation under vacuum ($\sim 10^{-5}$ Torr), with the ionized fragments detected by time-of-flight mass spectroscopy. The species identified were sulfur, $CHMe_2$, SO, CS_2, ZnS, a xanthate ligand, three-coordinate $Zn(S_2COCHMe_2)S$, and the parent compound $Zn(S_2COCHMe)_2$. The presence of the ligand and a three-coordinate species support the feasibility of processes A and E in Figure 6, which is consistent with the electron ionization mass data. The major fragments such as sulfur, propane, CS_2, and ZnS are the expected products of the various pathways in Figure 6.

The organic byproducts collected in a liquid nitrogen trap during the photo-CVD process are RH, ROH, CS_2, OCS, R−S−R, and RSH ($R = -CHMe_2$). The presence of RH and ROH supports Paths C and G. Direct C−OR dissociation from the parent molecule may also occur. Similarly, CS_2 and OCS are the byproducts of Paths C and G. The reactive ROCS• radical easily dissociates to give stable species such as OCS and RH, the latter of which is formed by R• abstracting a hydrogen from its surroundings (Path G). It is believed that the other alkyl containing sulfur species (RSH, and R−S−R) were formed via reactive radicals such as R• and S•.[34]

All of the species identified by mass spectroscopic data and by trapping the organic byproducts during the photolytic CVD process are consistent with metal−ligand dissociation and C−S bond and C−OR bond cleavage. The reactions shown in Figure 6 lead to the various organic species identified as well as to inorganic ZnS.

Conclusions

We demonstrate that hexagonal phase pure ZnS films can be prepared photochemically under mild conditions (e.g. low temperature) from a single source precursor with purity comparable to that of thermally grown films. Also, it is of interest that the deposits are obtained only on a selected area of the substrate irradiated by the laser beam.

(34) Similar explanations also have been reported on radical species of other chalcogene elements. (a) Henriksen, L. In *The Chemistry of Organic Selenium and Tellurium Compounds*; Patai, S., Ed.; Wiley: New York, 1987; Vol. 2. (b) Gysling, H. J.; Wernberg, A. A.; Blanton, T. N. *Chem. Mater*. **1992**, *4*, 900.

Our *in situ* gas-phase luminescence measurements show the presence of Zn atoms and S_2 in the gas phase during photodeposition. The results indicate that the deposition process depends on the absorption of light and involves a photochemical component in addition to possible surface adsorption of a photointermediate followed by further thermally catalyzed and photocatalyzed processes on the substrate surface.

Acknowledgment. This work was supported by the National Science Foundation (CHE-9509275). We thank James Ren (UCLA) for the XPS analyses and Dr. Kin-Man Yu (Lawrence Berkeley National Laboratory) for RBS measurements of the samples.

JA9625891